Efficient and Stable Inverted Wide-Bandgap Perovskite Solar Cells and Modules Enabled by Hybrid Evaporation-Solution Method

Amir Zarean Afshord, Bahri Eren Uzuner, Wiria Soltanpoor, Salar H. Sedani, Tom Aernouts, Gorkem Gunbas,* Yinghuan Kuang,* and Selcuk Yerci*

Wide-bandgap perovskite solar cells (WBG-PSCs), when partnered with Si bottom cells in tandem configuration, can provide efficiencies up to 44%; yet, the development of stable, efficient, and scalable WBG-PSCs is required. Here, the utility of the hybrid evaporation-solution method (HESM) is investigated to meet these demanding requirements via its unique advantages including ease of control and reproducibility. A PbI_2/CsBr layer is co-evaporated followed by coating of organic-halide solutions in a green solvent. Bandgaps between 1.55–1.67 eV are systematically screened by varying CsBr and MABr content. Champion efficiencies of 21.06% and 20.35% in cells and 19.83% and 18.73% in mini-modules (16 cm²) for perovskites with 1.64 and 1.67 eV bandgaps are achieved, respectively. Additionally, 18.51%-efficient semi-transparent WBG-PSCs are implemented in 4T perovskite/bifacial silicon configuration, reaching a projected power output of 30.61 mW cm⁻² based on PD IEC TS 60904-1-2 (BiFi200) protocol. Despite similar bandgaps achieved by incorporating Br via MABr solution and/or CsBr evaporation, PSCs having a perovskite layer without MABr addition show significantly higher thermal and moisture stability. This study proves scalable, high-performance, and stable WBG-PSCs are enabled by HESM, hence their use in tandems and in emerging applications such as indoor photovoltaics are now within reach.

1. Introduction

Perovskite solar cells (PSCs) have recently established a pivotal role in photovoltaics research community due to their high absorption coefficient, long carrier diffusion lengths, and bandgap tunability.[1–3] The rapid increase in their power conversion efficiency (PCE) from 3.8% to 25.7% has positioned them as a potential rival to compete with conventional photovoltaic materials.[4] Additionally, the bandgap tunability makes them suitable candidates to be utilized in various applications. In this regard, wide-bandgap perovskites, enabled mainly by inorganic cations and/or smaller halides compared to iodide have drawn significant attention as they bear great promise for tandem solar cells, indoor light conversion, and semi-transparent PSCs for building integration.[5–7] Particularly, PSCs with a bandgap near 1.7 eV are ideal for 2-terminal monofacial and 4-terminal bifacial tandem solar cells when coupled with silicon bottom cells.[8,9]

A. Z. Afshord, B. E. Uzuner, S. H. Sedani, G. Gunbas, S. Yerci
The Center for Solar Energy Research and Applications (ODTU-GUNAM)
Middle East Technical University
Ankara 06800, Turkey
E-mail: ggunbas@metu.edu.tr; syerci@metu.edu.tr

A. Z. Afshord, B. E. Uzuner, G. Gunbas, S. Yerci
Department of Micro and Nanotechnology
Middle East Technical University
Ankara 06800, Turkey

A. Z. Afshord, B. E. Uzuner
Thin Film PV Technology – Partner in Solliance
imec, 3600 Genk, Belgium

The ORCID identification number(s) for the author(s) of this article can be found under https://doi.org/10.1002/adfm.202301695.

A. Z. Afshord, B. E. Uzuner, T. Aernouts, Y. Kuang
EnergyVille
imo-imomec
Thor Park 8320, Genk 3600, Belgium
E-mail: yinghuan.kuang@imec.be

A. Z. Afshord, B. E. Uzuner
Department of Electrical Engineering (ESAT)
Katholieke Universiteit Leuven
3001 Leuven, Belgium

W. Soltanpoor
MESA+ Institute for Nanotechnology
University of Twente
Enschede 7500 AE, the Netherlands

T. Aernouts, Y. Kuang
Imec, imo-imomec
Thin Film PV Technology – partner in Solliance
Thor Park 8320, 3600 Genk, Belgium

T. Aernouts, Y. Kuang
Hasselt University
imo-imomec
Martelarenlaan 42, 3500 Hasselt, Belgium

In this regard, efficiencies as high as 19.1% have already been reached for a perovskite with 1.74 eV bandgap.[10] Despite the improved device performance, stability, and bandgap tunability, wide-bandgap perovskite solar cells (WBG-PSCs) achieved by Br incorporation often suffer from light-induced phase segregation of iodine- and bromine-rich domains when the bandgap is above 1.69 eV.[11,12] Such issues can be circumvented by detailed compositional optimizations and/or additive engineering.[13] For example, introducing inorganic CsX (X = Br, I) into perovskite improves cell photostability and carrier lifetime, and reduces carrier recombination.[14,15] The amount of introduced Cs is critical; while it can stabilize the perovskite phase by reducing Gibbs free energy,[16] lower trap states density,[17] and enhance photogenerated carrier lifetime,[18] excess Cs could result in increased defect density and phase segregation.[19,20] Also, methyl ammonium salts, such as MACl and MABr, are crucial additives to enhance perovskite film crystallinity thus resulting in improved performance and more importantly phase stability.[21]

To date, the most efficient PSCs have been prepared by the spin-coating technique.[22,23] Despite the ease and success of spin-coating in demonstrating proof-of-concept studies on efficient PSCs, it is not considered a scalable technique mainly due to its sensitivity to processing conditions and size limitations.[24] Furthermore, it is not straightforward to use this technique for conformal and uniform film deposition on textured surfaces.[5] In contrast, vacuum deposition showed uniform and precise control on film thickness, representing compatible deposition with scalable fabrication on rough surfaces.[25] However, the performance of evaporated multi-cation perovskites lags behind the solution-processed counterparts due to the complications that arise from varying vapor pressures of multiple different source materials that result in complexity in tuning deposition rates.[26] Nevertheless, sequential vacuum deposition, where inorganic (PbX_2 and CsX) precursors are evaporated followed by organic precursor evaporation, is proved promising to fabricate uniform and large area solar cells with high reproducibility, high efficiency and stability.[27] An alternative approach is the hybrid evaporation-solution method (HESM), where the inorganic components (PbX_2 and CsX) are vapor-deposited, followed by solution-processing of multi-organic counterparts.[28,29] The perovskite layer is formed by the volume expansion of evaporated inorganic compounds via introducing the organic solution, which results in uniform and pinhole-free perovskite films.[30–32] This method is thickness-controlled and compatible with tandem cells with textured bottom Si cells as the first layer is vapor-processed.[28,33–36] Additionally, the composition can be controlled with ease and accuracy thanks to the solution-based second step. The flexibility of the precursor introduction via vapor or solution step provides a large window of parameters for bandgap tunability and structural control. Recently, Tan et al. reported 24.3% efficient and stable perovskite solar cells and 16 cm² mini-module with PCE of 20.0% using a sequential vapor-solution method in nip configuration.[37] Another combined sequential approach is the solution-vapor method, where inorganic precursors are spin-coated, followed by evaporated organic components. Wang et al. have reported MA-free nip perovskite with sequential solution-vapor method, where inorganic precursors are solution deposited, following vapor-deposited FAI, and achieved over 24% of PCE and high moisture stability.[38]

Here, we report a systematic study involving 35 sets of perovskite compositions aimed at achieving efficient, stable, and scalable wide-bandgap PSCs by the HESM. PbI_2 and CsBr were co-evaporated and followed by spin-coating a solution with formamidinium- (FA) and methylammonium (MA)-halide to form perovskite films. We optimized CsBr rate and MABr concentration and achieved champion small-area opaque PSCs with 21.06% and 20.35% PCE; semi-transparent PSCs with 18.30% and 18.51% PCE and mini-modules (active area of 15.36 cm²) with 19.83% and 18.73% PCE for perovskites having bandgaps of 1.64 and 1.67 eV, respectively. A power output of 30.61 mW cm^{-2} is demonstrated by utilizing semi-transparent PSCs in 4T perovskite/bifacial silicon configuration (industrial BiFi PERC cell). Finally, we demonstrated that WBG-PSCs in which Br incorporation was achieved by evaporation of CsBr can retain over 80% PCE for 2500 h under thermal stress (85 °C) and 1600 h at ≈50% relative humidity significantly outperforming the cells where Br incorporation achieved in solution phase with MABr. We revealed trade-offs for adding Br via solution and/or evaporation to achieve high bandgap, PCE, and stability at the same time. Precise sweeping CsBr evaporation rate and MABr concentration in this hybrid method allows the fine tuning of CsBr and MABr contents in the perovskite films, resulting in inverted WBG-PSCs and mini-modules on bare sputtered NiOx with high efficiency and stability. Also, high GFF of 96% and minor upscaling losses are demonstrated for the minimodules, with the module efficiency among the highest values in the literature with bandgap over 1.60 eV.

2. Results and Discussion

Cs and Br concentrations were controlled toward facilitating wide-bandgap perovskite compositions by evaporating CsBr and incorporating MABr into the organic solution together with FAI and MACl. PSCs with different perovskite compositions were fabricated in the p-i-n configuration with the architecture of MgF₂/Glass/ITO/NiOx/Perovskite/LiF/C₆₀/BCP/Cu (**Figure 1**a, device fabrication details are given in supporting information). Large monolithic grains from the bottom to the top of the perovskite films were attained. A representative cross-sectional scanning electron microscopy (SEM) image of perovskite deposited at 1.2 Å s^{-1} CsBr rate is shown in Figure 1b. The impact of CsBr rates and MABr concentrations on PCE of PSCsperovskite bandgap and PCE of PSCs, extracted

G. Gunbas
Department of Polymer Science and Technology
Middle East Technical University
Ankara 06800, Turkey

G. Gunbas
Department of Chemistry
Middle East Technical University
Ankara 06800, Turkey

S. Yerci
Department of Electrical and Electronics Engineering
Middle East Technical University
Ankara 06800, Turkey
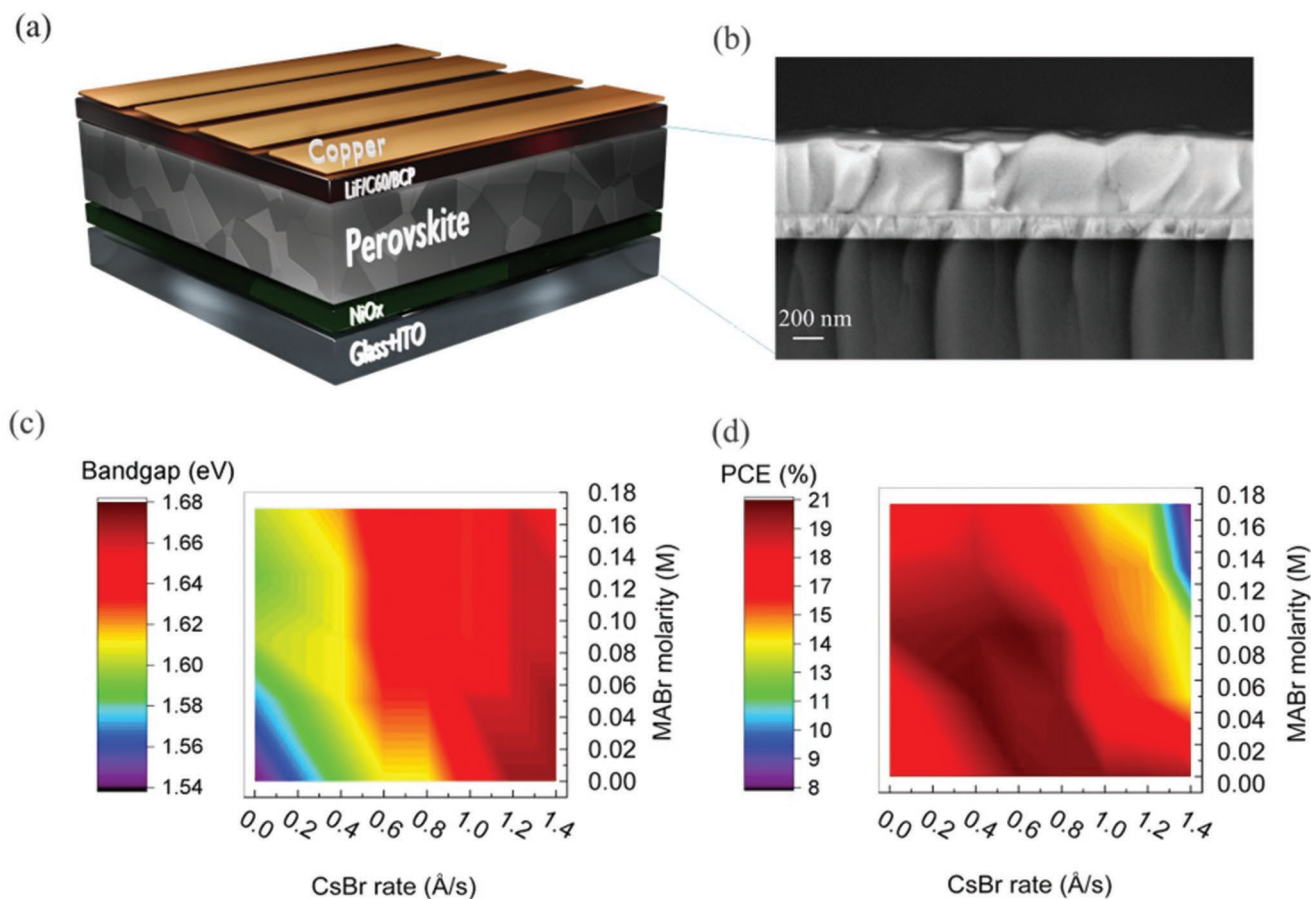
Figure 1. a) Schematic of the solar cell structure, b) cross-sectional SEM image of the perovskite layer deposited on NiOx/ITO/glass substrate. Color-maps of c) perovskite bandgap, and d) PCE.
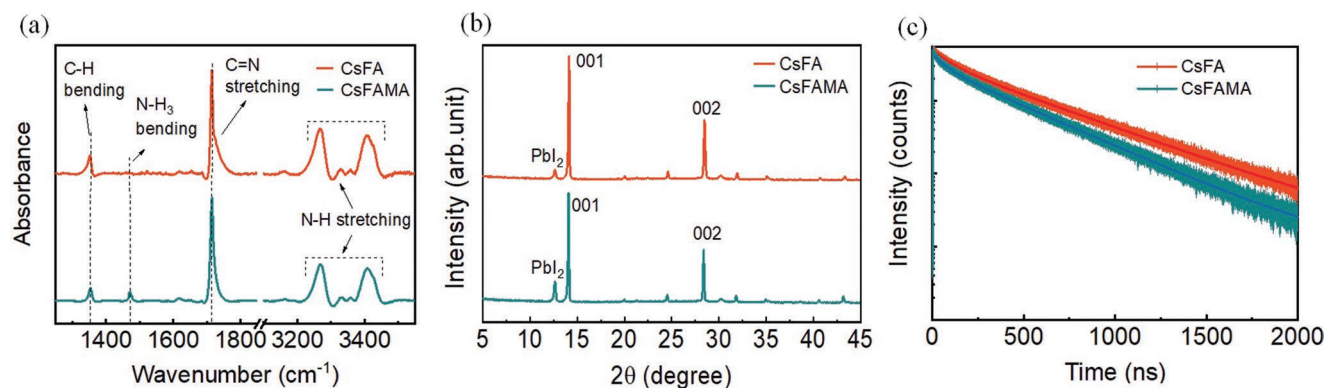
from Photoluminescence (PL) spectra (Figure S1, Supporting Information) and J–V curves (Figure S2, Supporting Information), are illustrated in Figures 1c,d, respectively. The device performance parameters are provided in Table S1 (Supporting Information). For the perovskite films with no MABr addition, the bandgap steadily increases with the CsBr incorporation, reaching a value of ≈1.67 eV at the 1.2 Å s^{-1} CsBr rate. Additionally, cell efficiencies increase with CsBr rate up to 0.6 Å s^{-1} and slightly reduce thereafter. MABr incorporation enlarges the bandgap of perovskite for low CsBr rates (up to 0.6 Å s^{-1}); however, it does not significantly affect it at higher CsBr rates. An optimum region for MABr concentration and CsBr rate that enables high performance (>19%)

PSCs. For CsBr rates of 0.8 Å s^{-1} and below, the optimum MABr concentration is found to be ≈0.09 м. For higher CsBr rates, the addition of MABr into the solution has detrimental effects on the performance of PSCs.

Based on the aforementioned systematic optimization of CsBr rate and MABr concentration on perovskite bandgap and device performance, hereafter, we focused our investigations on the two perovskite compositions: 1) CsBr rate of 0.6 Å s^{-1} and MABr concentration of 0.09 м provides a champion PCE of 21.06% at 1.64 eV bandgap (CsFAMA), and 2) CsBr rate of 1.2 Å s^{-1} with no MABr enables a PCE of 20.34% at the largest investigated bandgap of 1.67 eV (CsFA). Fourier transform

infrared spectroscopy (FTIR) was performed to identify the chemical identity of these two perovskite layers (**Figure 2**a). Both films showed peaks at 1712 and 1354 cm^{-1} belonging to C=N symmetric stretching and C−H bending of FA$^+$ cation, respectively.[39,40] Importantly, the bending peak of NH$_3$ at 1472 cm^{-1} — representing MA$^+$ cation — is only present for perovskite with MABr addition (CsFAMA) but not in CsFA, justifying the abbreviations. It is important to note here that the solution phase for the preparation of CsFA contained MA cations (half the concentration of CsFAMA) as MACl. The lack of MA upon MACl addition into perovskite is extensively discussed in the literature.[41,42] X-ray diffractograms of CsFA and CsFAMA films are nearly identical and represent the black perovskite phase; yet, CsFAMA has a larger PbI$_2$ peak, indicating a higher fraction of unreacted PbI$_2$ (Figure 2b). PL studies revealed relatively long average PL lifetimes (Equations S1,S2, Supporting Information) are achieved for both CsFAMA (393 ns) and CsFA (450 ns) (Figure 2c).[43–45]

EQE values for opaque PSCs in the spectrum range of ≈400–750 nm are ≈95% (CsFAMA) and 90% (CsFA), indicating an excellent charge extraction (**Figure 3**a). The bandgaps of CsFAMA and CsFA are found as 1.64 and 1.67 eV from the peaks of the Gaussian-fitted differentiated-EQE spectra (Figure 3a) and are consistent with the PL measurements (Figure S1, Supporting Information). The average efficiencies of CsFAMA and

**ADVANCED
SCIENCE NEWS**

www.advancedsciencenews.com

**ADVANCED
FUNCTIONAL
MATERIALS**

www.afm-journal.de

Figure 2. a) FTIR spectra, b) X-ray diffraction patterns, and c) Time-resolved PL decay curves for CsFAMA and CsFA perovskite films.

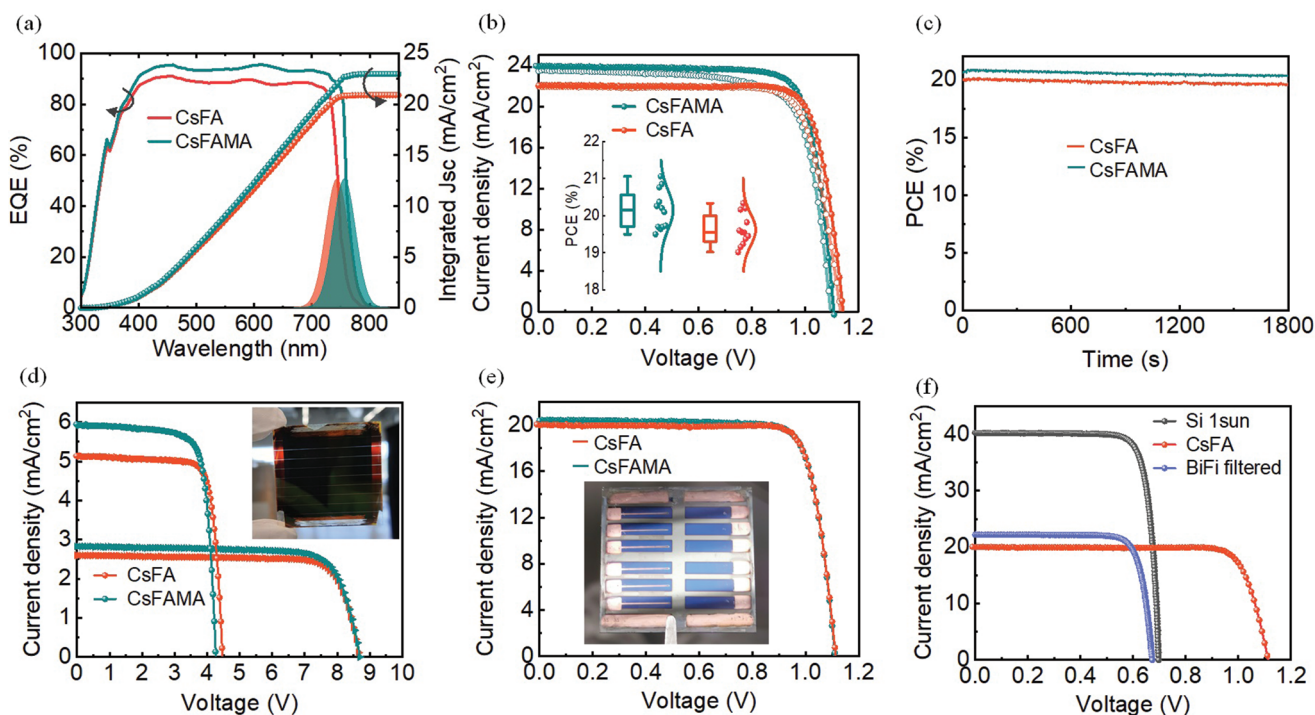CsFA PSCs are 20.17±0.48% and 19.61±0.37% based on the statistics (12 cells) shown in the insets of Figure 3b. Small deviations indicate high layer uniformity and reproducibility of the process. Additionally, the CsFA PSCs possess low hysteresis indices (HI) (Equation S3, Supporting Information) of 3.8%, whereas the CsFAMA PSCs demonstrate a higher HI of 7.7%, as shown in Figure 3b and Table S2 (Supporting Information). The lower HI obtained in CsFA PSCs is due to smaller defect density and less residual PbI₂ revealed by a slightly longer PL lifetime and slightly narrower XRD peak for perovskite, and a less intense XRD peak for PbI₂. A relatively large HI is associated with the lack of a passivation layer on NiOx.[46–48] Stabilized cell efficiencies of 20.33% and 19.55% are attained for opaque CsFAMA and CsFA PSCs, respectively, under continuous illumination after 1800 s. Less than 2% relative efficiency decrease was observed for both CsFAMA and CsFA PSCs as shown in Figure 3c.

To demonstrate the scalability of HESM, we fabricated perovskite solar modules (PSMs) with aperture areas of 4 and 16 cm² (Figure S3, Supporting Information), consisting of 4 and 8 interconnected cells, respectively. A very high geometric fill factor (GFF) of 96% (Figure S3, Supporting Information) with PCEs of 19.83% (20.43%) for CsFAMA and 18.73% (19.09%) for CsFA PSMs were achieved with an active area of 15.36 cm² (3.84 cm²) as shown in Figure 3d and Table S3 (Supporting Information). To our best knowledge, these efficiency values are among the highest reported for wide-bandgap (>1.6 eV) PSMs in the literature for their respective areas.[49] Remarkably, only 2% absolute PCE loss was achieved upon upscaling from small area cells to modules of 8 cells.[50]

To demonstrate the potential utilization of perovskite by HESM in perovskite/silicon tandem solar cells, semi-transparent PSCs with the architecture of MgF₂/Glass/ITO/NiOx/Perovskite/LiFx/C₆₀/BCP/ITO were also fabricated and efficiencies of 18.22% (CsFAMA) and 18.51% (CsFA) were achieved for the champion PSCs (Figure 3e; Table S4, Supporting Information). While short-circuit current density (Jsc) for both perovskites are lower compared to their opaque counterparts as the rear side lacks a metal reflector, no notable fill factor (FF) and open circuit voltage (Voc) losses were observed. These results culminated in only 2% absolute efficiency loss when average PCEs for semi-transparent and opaque PSCs are compared. Next, we utilized the semi-transparent CsFA

(due to its higher efficiency and bandgap) in perovskite/bifacial silicon tandem solar cells. Commercial bifacial Si solar cells with 22.58% efficiency and 77.9 % bifaciality were utilized. The power output of the tandem device was obtained based on PD IEC TS 60904-1-2 (BiFi200) protocol and the method developed by Zhang et al. which is provided in supporting information.[51,52] In addition to 18.51 mW cm⁻² produced by semi-transparent CsFA PSCs, filtered Si BiFi solar cell generated 12.10 mW cm⁻², summing up a power output of 30.61 mW cm⁻² (Figure 3f).

Finally, we performed thermal, moisture, shelf, and phase stability tests for both perovskite compositions (**Figure 4**). For thermal stability test, unencapsulated solar cells with top ITO contact were kept on the hotplate at 85 °C inside N₂-filled glovebox. Also, for moisture stability test, solar cells with ITO top contact without any encapsulation were kept in ambient air with relative humidity of ≈50%. For shelf-stability test, opaque solar cells were stored inside N₂-filled glovebox for 1440 h. The J–V measurements were carried out inside N₂-filled glovebox for both stability tests. Thermal stability studies revealed that the efficiency of the semi-transparent CsFAMA PSCs dropped to 77% of its initial efficiency after 400 h. Notably, CsFA PSCs retained 80% of their initial efficiency (T₈₀) after 2560 h (Figure 4a), which is among the most stable PSCs reported in the literature, especially when wide-bandgap PSCs are concerned (≈1.67 eV). Although relatively faster degradation of PSCs for both compositions was observed in the humidity test, CsFA still strongly outperformed the CsFAMA counterpart. CsFAMA PSCs dropped to 67% of their initial efficiency after 170 h, while CsFA PSCs retained 80% of their initial efficiency after 1600 h (Figure 4a). Finally, the phase stability of both perovskites in MgF₂/Glass/ITO/NiOx/Perovskite/LiFx/C₆₀/BCP device structure under continuous laser illumination at 532 nm in the ambient atmosphere (≈50% RH) was investigated. As the shape of PL spectra remains symmetric and unchanged upon laser excitation (Figure S4, Supporting Information), it implies that both perovskite compositions have a stable phase without halide redistribution.[53] While the structure with CsFA PSCs does not undergo a shift or significant intensity change (<10%), that with CsFAMA exhibits a spectral red-shift (≈5 nm) and substantial intensity change of over 200% (Figure 4b). The red-shift and increased PL intensity are generally attributed

ADVANCED
SCIENCE NEWS
www.advancedsciencenews.com

ADVANCED
FUNCTIONAL
MATERIALS
www.afm-journal.de

Perovskite	Small Area cell (0.125 cm²) (%)	Module (4 cm²) (%)	Module (16 cm²) (%)	Semi-trans. cell (0.125 cm²) (%)	Tandem (with Bifi200) (mW/cm²)
CsFAMA	21.06	20.34	19.83	18.30	
CsFA	20.35	19.09	18.73	18.51	30.61

Figure 3. a) EQE and d(EQE)/dλ spectra, and integrated Jsc, b) Reverse and forward J–V curves and c) Maximum power point tracking PCE versus time plots of CsFAMA and CsFA solar cells. d) J–V curves of opaque mini-modules on 4 cm² (sphere) and 16 cm² (triangle) aperture areas with 96% GFF for CsFAMA and CsFA. The inset photograph in (d) shows a 16 cm² opaque CsFAMA perovskite mini-module (glass side view). e) J–V curves for semi-transparent solar cells for CsFA and CsFAMA. The inset in (e) is a picture of semi-transparent CsFA solar cell (the rear side view). f) J–V curves of Si and semi-transparent perovskite (CsFA) solar cells under 1-sun, and J–V curve of Si solar cell measured by filter under BiFi 200 condition. The cut-off wavelengths are extracted from d(EQE)/dλ spectra in (a). PCE statistical distribution of 12 pixels cells are given in the inset of (b).

to photoinduced lattice expansion toward enhanced symmetry which leads to a reduction of trap density and suppresses non-radiative recombination sites.[53]

Several seminal works have clearly demonstrated the beneficial and detrimental effects of i) residual PbI_2 on perovskite surface,[54] ii) Cs content,[17–19] and iii) MA incorporation in perovskite compositions.[55–57] To elucidate the origin of the notable difference in thermal and humidity stability between CsFAMA and CsFA, we performed detailed PL and FTIR studies (Figure 4c,d). PL spectra of CsFAMA after thermal and moisture tests (500 h) revealed a shoulder ≈720 nm which is typically associated with halide segregation.[58,59] PL peaks of both compositions shift to lower energies upon humidity test, which can be attributed to the formation of localized traps due to interaction with water molecules perovskite's organic components as films are unencapsulated.[60–62] PL peaks of

CsFA remained symmetric and underwent a minimal intensity change, in accord with its superior stability. As no MA^+ was detected in FTIR for CsFA (Figure 2a), we performed FTIR spectroscopy measurement for CsFAMA samples after heat and humidity tests (up to 500 h) (Figure S5, Supporting Information). The intensity ratio of the NH_3 bending and C—H stretching bands upon thermal and humidity tests reaches 10% of the initial value only after 1000 and 10 mins, respectively (Figure 4d). Thus, we believe phase segregation for CsFAMA is most probably related to the fast release of MA in this composition. Here, we successfully demonstrated that the introduction of MA via MACl in solution and incorporation of Br via CsBr evaporation[63] decouples the MA introduction (as an additive) and Br incorporation and is among the best strategies toward achieving high performance, stable wide band-gap perovskites for tandem applications.
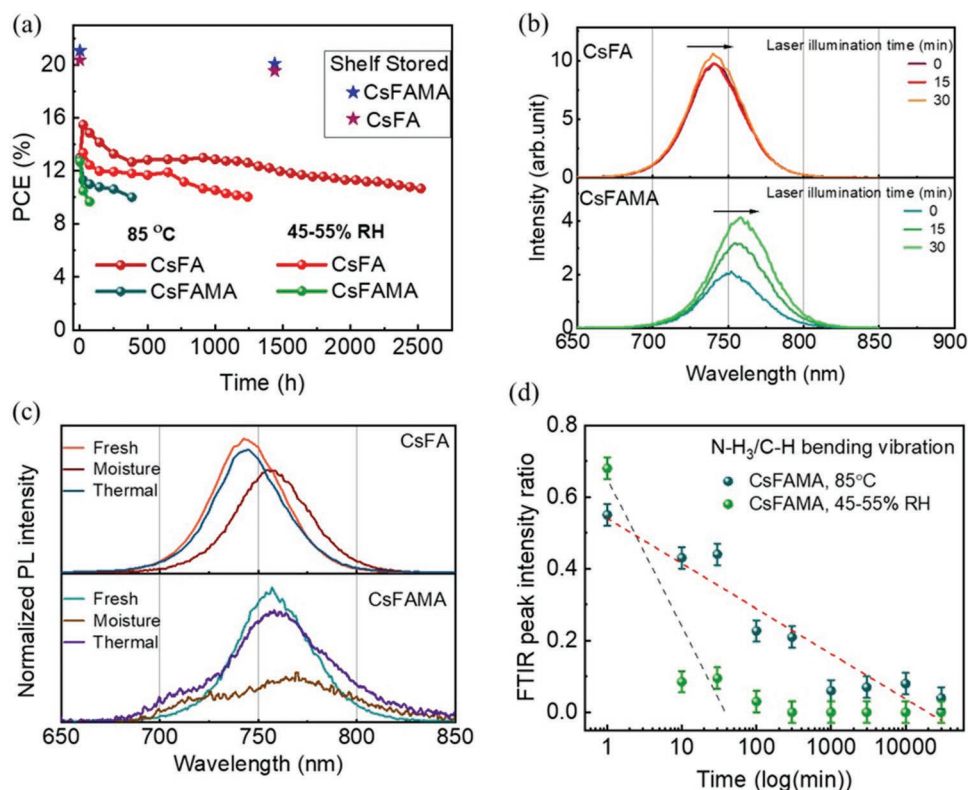
Figure 4. a) The evolution of PCE versus time for CsFA and CsFAMA solar cells during thermal (85 °C) in an inert atmosphere and humidity (relative humidity in the range of ≈50%) stability tests in air. PCE was traced until it reduced to <80% of its initial value (T_{80}) and shelf-stability tracking of solar cells stored inside the N_2-filled golvebox for 1440 h. b) PL spectra of CsFA and CsFAMA in the MgF_2/Glass/ITO/NiO_x/Perovskite structure upon excitation. c) PL spectra of CsFA and CsFAMA before and after thermal and moisture stress for 500 h. Peaks are normalized to fresh sample's peak intensity. d) FTIR peaks (N-H_3/C-H bending vibration) intensity ratio versus time for films with CsFA and CsFAMA perovskite films during thermal and humidity stability tests.

3. Conclusion

In conclusion, we demonstrated high-performance wide-bandgap PSCs in the p-i-n configuration with light, thermal, moisture and phase stability by tuning the CsBr rate in the PbI_2-CsBr co-evaporation, and MABr concentration of HESM. We achieved 21.06% PCE at 1.64 eV bandgap for CsFAMA and 20.34% PCE at 1.67 eV bandgap for CsFA-based PSCs. We fabricated solar modules with active areas of 3.84 and 15.36 cm^2 to prove the scalability and achieved PCEs of 20.34% and 19.83% (CsFAMA) and those of 19.09% and 18.73% (CsFA), respectively, with <2% absolute efficiency loss compared to small area opaque champion cells. Semi-transparent PSCs with PCEs of 18.22% and 18.51% for CsFAMA and CsFA were fabricated. Additionally, 30.61 mW cm^{-2} power output was demonstrated in 4T perovskite/bifacial silicon tandem solar cell geometry.

Finally, we disclosed that a longer carrier lifetime (450 versus 393 ns), smaller HI (3.8% versus 7.7%), higher stability during humidity (80% of its initial PCE (T_{80}) at 2560 versus 400 h) and heat (T_{80} at 1600 versus 170 h) tests, and smaller spectral shift (0 versus 5 nm) with light exposure in PSCs are attained with perovskites fabricated via Br incorporation by CsBr-only (CsFA). These superior properties are associated with less defects, less residual PbI_2, higher Cs content

and controlled MA incorporation mechanism that together resulted in better crystallinity.

Overall, Br introduction via CsBr with HESM has been demonstrated to be the key approach for the realization of wide-bandgap perovskite for tandem solar cells and other emerging applications such as indoor photovoltaics.

Supporting Information

Supporting Information is available from the Wiley Online Library or from the author.

Acknowledgements

Conflict of Interest

The authors declare no conflict of interest.

Data Availability Statement

The data that support the findings of this study are available in the supplementary material of this article.

Keywords

4-terminal tandem solar cells, hybrid deposition methods, perovskite solar cells and modules, scalability, stability, thermal co-evaporation, wide-bandgap perovskites

[1] H. J. Snaith, *J. Phys. Chem. Lett.* **2013**, *4*, 3623.
[2] S. D. Stranks, G. E. Eperon, G. Grancini, C. Menelaou, M. J. P. Alcocer, T. Leijtens, L. M. Herz, A. Petrozza, H. J. Snaith, *Science.* **2013**, *342*, 341.
[3] M. R. Filip, G. E. Eperon, H. J. Snaith, F. Giustino, *Nat. Commun.* **2014**, *5*, 5757.
[4] NREL, Best Research-Cell Efficiencies, https://www.nrel.gov/pv/cell-efficiency.html (accessed: Febrary 10 2022).
[5] J. Werner, B. Niesen, C. Ballif, *Adv. Mater. Interfaces* **2018**, *5*, 1700731.
[6] Y. Li, R. Li, Q. Lin, *Small* **2022**, *18*, 1.
[7] G. Giuliano, A. Bonasera, G. Arrabito, B. Pignataro, *Sol. RRL* **2021**, *5*, 2100702.
[8] M. De Bastiani, A. J. Mirabelli, Y. Hou, F. Gota, E. Aydin, T. G. Allen, J. Troughton, A. S. Subbiah, F. H. Isikgor, L. Liu, L. Xu, B. Chen, E. Van Kerschaver, D. Baran, B. Fraboni, M. F. Salvador, U. W. Paetzold, E. H. Sargent, S. De Wolf, *Nat. Energy* **2021**, *6*, 167.
[9] M. T. Hörantner, H. J. Snaith, *Energy Environ. Sci.* **2017**, *10*, 1983.
[10] H. Tan, F. Che, M. Wei, Y. Zhao, M. I. Saidaminov, P. Todorović, D. Broberg, G. Walters, F. Tan, T. Zhuang, B. Sun, Z. Liang, H. Yuan, E. Fron, J. Kim, Z. Yang, O. Voznyy, M. Asta, E. H. Sargent, *Nat. Commun.* **2018**, *9*, 9.
[11] E. T. Hoke, D. J. Slotcavage, E. R. Dohner, A. R. Bowring, H. I. Karunadasa, M. D. McGehee, *Chem. Sci.* **2015**, *6*, 613.
[12] U. C. Gupta, *Inf. Syst. Manag.* **1992**, *9*, 28.
[13] R. J. Stoddard, A. Rajagopal, R. L. Palmer, I. L. Braly, A. K. Y. Jen, H. W. Hillhouse, *ACS Energy Lett.* **2018**, *3*, 1261.
[14] K. A. Bush, K. Frohna, R. Prasanna, R. E. Beal, T. Leijtens, S. A. Swifter, M. D. McGehee, *ACS Energy Lett.* **2018**, *3*, 428.
[15] T. Liu, H. Lai, X. Wan, X. Zhang, Y. Liu, Y. Chen, *Chem. Mater.* **2018**, *30*, 5264.
[16] L. T. Schelhas, Z. Li, J. A. Christians, A. Goyal, P. Kairys, S. P. Harvey, D. H. Kim, K. H. Stone, J. M. Luther, K. Zhu, V. Stevanovic, J. J. Berry, *Energy Environ. Sci.* **2019**, *12*, 1341.
[17] J. W. Lee, D. H. Kim, H. S. Kim, S. W. Seo, S. M. Cho, N. G. Park, *Adv. Energy Mater.* **2015**, *5*, 1501310.
[18] M. Saliba, T. Matsui, J. Y. Seo, K. Domanski, J. P. Correa-Baena, M. K. Nazeeruddin, S. M. Zakeeruddin, W. Tress, A. Abate, A. Hagfeldt, M. Grätzel, *Energy Environ. Sci.* **2016**, *9*, 1989.
[19] S. Tang, S. Huang, G. J. Wilson, A. Ho-Baillie, *Trends Chem* **2020**, *2*, 638.
[20] F. W. Jones, W. L. Bragg, *Proc. R. Soc. London. Ser. A. Math. Phys. Sci.* **1938**, *166*, 16.
[21] F. Zhang, K. Zhu, *Adv. Energy Mater.* **2020**, *10*, 1902579.
[22] H. Min, D. Y. Lee, J. Kim, G. Kim, K. S. Lee, J. Kim, M. J. Paik, Y. K. Kim, K. S. Kim, M. G. Kim, T. J. Shin, S. Il Seok, *Nature* **2021**, *598*, 444.
[23] Q. Jiang, J. Tong, Y. Xian, R. A. Kerner, S. P. Dunfield, C. Xiao, R. A. Scheidt, D. Kuciauskas, X. Wang, M. P. Hautzinger, R. Tirawat, M. C. Beard, D. P. Fenning, J. J. Berry, B. W. Larson, Y. Yan, K. Zhu, *Nature* **2022**, *611*, 278.
[24] J. Kim, J. S. Yun, Y. Cho, D. S. Lee, B. Wilkinson, A. M. Soufiani, X. Deng, J. Zheng, A. Shi, S. Lim, S. Chen, Z. Hameiri, M. Zhang, C. F. J. Lau, S. Huang, M. A. Green, A. W. Y. Ho-Baillie, *ACS Energy Lett.* **2017**, *2*, 1978.
[25] I. Susic, L. Gil-Escrig, F. Palazon, M. Sessolo, H. J. Bolink, *ACS Energy Lett.* **2022**, *7*, 1355.
[26] T. Gallet, R. G. Poeira, E. M. Lanzoni, T. Abzieher, U. W. Paetzold, A. Redinger, *ACS Appl. Mater. Interfaces* **2021**, *13*, 2642.
[27] H. Li, J. Zhou, L. Tan, M. Li, C. Jiang, S. Wang, X. Zhao, Y. Liu, Y. Zhang, Y. Ye, W. Tress, C. Yi, *Sci Adv* **2022**, *8*, eabo7422.
[28] F. Sahli, J. Werner, B. A. Kamino, M. Bräuninger, R. Monnard, B. Paviet-Salomon, L. Barraud, L. Ding, J. J. Diaz Leon, D. Sacchetto, G. Cattaneo, M. Despeisse, M. Boccard, S. Nicolay, Q. Jeangros, B. Niesen, C. Ballif, *Nat. Mater.* **2018**, *17*, 820.
[29] W. Soltanpoor, C. Dreessen, M. C. Sahiner, I. Susic, A. Z. Afshord, V. S. Chirvony, P. P. Boix, G. Gunbas, S. Yerci, H. J. Bolink, *ACS Appl. Energy Mater.* **2020**, *3*, 8257.
[30] J. Burschka, N. Pellet, S. J. Moon, R. Humphry-Baker, P. Gao, M. K. Nazeeruddin, M. Grätzel, *Nature* **2013**, *499*, 316.
[31] Z. Li, T. R. Klein, D. H. Kim, M. Yang, J. J. Berry, M. F. A. M. Van Hest, K. Zhu, *Nat. Rev. Mater.* **2018**, *3*, 18017.
[32] J. H. Im, I. H. Jang, N. Pellet, M. Grätzel, N. G. Park, *Nat. Nanotechnol.* **2014**, *9*, 927.
[33] L. Mao, T. Yang, H. Zhang, J. Shi, Y. Hu, P. Zeng, F. Li, J. Gong, X. Fang, Y. Sun, X. Liu, J. Du, A. Han, L. Zhang, W. Liu, F. Meng, X. Cui, Z. Liu, M. Liu, *Adv. Mater.* **2022**, *34*, 2206193.
[34] S. W. Lee, S. Bae, J. K. Hwang, W. Lee, S. Lee, J. Y. Hyun, K. Cho, S. Kim, F. D. Heinz, S. Bin Choi, D. Choi, D. Kang, J. Yang, S. Jeong, S. J. Park, M. C. Schubert, S. Glunz, W. M. Kim, Y. Kang, H. S. Lee, D. Kim, *Commun Chem* **2020**, *3*, 37.
[35] CSEM, *EPFL achieve 31.25% efficiency for tandem perovskite-silicon solar cell – pv magazine International (pv-magazine.com)*.
[36] H. Li, M. Liu, M. Li, H. Park, N. Mathews, Y. Qi, X. Zhang, H. J. Bolink, K. Leo, M. Graetzel, C. Yi, *iEnergy* **2023**, *1*, 434.
[37] L. Tan, J. Zhou, X. Zhao, S. Wang, M. Li, C. Jiang, H. Li, Y. Zhang, Y. Ye, W. Tress, L. Ding, M. Grätzel, C. Yi, *Adv. Mater.* **2023**, *35*, 2205027.
[38] S. Wang, L. Tan, J. Zhou, M. Li, X. Zhao, H. Li, W. Tress, L. Ding, M. Graetzel, C. Yi, *Joule* **2022**, *6*, 1344.
[39] Z. Zhou, S. Pang, F. Ji, B. Zhang, G. Cui, *Chem. Commun.* **2016**, *52*, 3828.
[40] L. Q. Xie, T. Y. Zhang, L. Chen, N. Guo, Y. Wang, G. K. Liu, J. R. Wang, J. Z. Zhou, J. W. Yan, Y. X. Zhao, B. W. Mao, Z. Q. Tian, *Phys. Chem. Chem. Phys.* **2016**, *18*, 18112.
[41] A. Dualeh, N. Tétreault, T. Moehl, P. Gao, M. K. Nazeeruddin, M. Grätzel, *Adv. Funct. Mater.* **2014**, *24*, 3250.
[42] K. Odysseas Kosmatos, L. Theofylaktos, E. Giannakaki, D. Deligiannis, M. Konstantakou, T. Stergiopoulos, *Energy Environ. Mater* **2019**, *2*, 79.
[43] G. Han, H. D. Hadi, A. Bruno, S. A. Kulkarni, T. M. Koh, L. H. Wong, C. Soci, N. Mathews, S. Zhang, S. G. Mhaisalkar, *J. Phys. Chem. C* **2018**, *122*, 13884.
[44] B. Li, Y. Zhang, L. Fu, T. Yu, S. Zhou, L. Zhang, L. Yin, *Nat. Commun.* **2018**, *9*, 1076.
[45] J. Duan, Y. Zhao, B. He, Q. Tang, *Angew. Chemie* **2018**, *130*, 3849.
[46] A. Kumar, A. Rana, N. Vashistha, K. K. Garg, R. K. Singh, *Sol. Energy* **2020**, *211*, 345.

**ADVANCED
SCIENCE NEWS**

www.advancedsciencenews.com

**ADVANCED
FUNCTIONAL
MATERIALS**

www.afm-journal.de

[47] T. P. Gujar, T. Unger, A. Schönleber, M. Fried, F. Panzer, S. Van Smaalen, A. Köhler, M. Thelakkat, *Phys. Chem. Chem. Phys.* **2017**, *20*, 605.

[48] J. K. Kim, D. N. Nguyen, J. H. Lee, S. Kang, Y. Kim, S. S. Kim, H. K. Kim, *J. Alloys Compd.* **2020**, *818*, 152887.

[49] S. L. Hamukwaya, H. Hao, Z. Zhao, J. Dong, T. Zhong, J. Xing, L. Hao, M. M. Mashingaidze, *Perovskite Solar Cells* **2022**, *12*, 252.

[50] D. B. Ritzer, T. Abzieher, A. Basibüyük, T. Feeney, F. Laufer, S. Ternes, B. S. Richards, S. Bergfeld, U. W. Paetzold, *Prog. Photovoltaics Res. Appl.* **2022**, *30*, 360.

[51] X. Liu, Z. Wu, X. Fu, L. Tang, J. Li, J. Gong, X. Xiao, *Nano Energy* **2021**, *86*, 106114.

[52] D. Zhang, W. Verhees, M. Dörenkämper, W. Qiu, K. Bakker, A. Gutjahr, S. Veenstra, R. Gehlhaar, U. W. Paetzold, W. Soppe, I. Romijn, L. J. Geerligs, T. Aernouts, A. Weeber, *Energy Procedia* **2016**, *92*, 669.

[53] H. S. Kim, A. Hagfeldt, *Adv. Opt. Mater.* **2019**, *7*, 1801512.

[54] F. Liu, Q. Dong, M. K. Wong, A. B. Djurišić, A. Ng, Z. Ren, Q. Shen, C. Surya, W. K. Chan, J. Wang, A. M. C. Ng, C. Liao, H. Li, K. Shih, C. Wei, H. Su, J. Dai, *Adv. Energy Mater.* **2016**, *6*, 1502206.

[55] B. Conings, J. Drijkoningen, N. Gauquelin, A. Babayigit, J. D'Haen, L. D'Olieslaeger, A. Ethirajan, J. Verbeeck, J. Manca, E. Mosconi, F. De Angelis, H. G. Boyen, *Adv. Energy Mater.* **2015**, *5*, 1500477.

[56] J. Yang, X. Liu, Y. Zhang, X. Zheng, X. He, H. Wang, F. Yue, S. Braun, J. Chen, J. Xu, Y. Li, Y. Jin, J. Tang, C. Duan, M. Fahlman, Q. Bao, *Nano Energy* **2018**, *54*, 218.

[57] E. J. Juarez-Perez, Z. Hawash, S. R. Raga, L. K. Ono, Y. Qi, *Energy Environ. Sci.* **2016**, *9*, 3406.

[58] Z. Andaji-Garmaroudi, M. Abdi-Jalebi, D. Guo, S. Macpherson, A. Sadhanala, E. M. Tennyson, E. Ruggeri, M. Anaya, K. Galkowski, R. Shivanna, K. Lohmann, K. Frohna, S. Mackowski, T. J. Savenije, R. H. Friend, S. D. Stranks, *Adv. Mater.* **2019**, *31*, 1902374.

[59] A. J. Knight, J. Borchert, R. D. J. Oliver, J. B. Patel, P. G. Radaelli, H. J. Snaith, M. B. Johnston, L. M. Herz, *ACS Energy Lett.* **2021**, *6*, 799.

[60] J. M. Howard, E. M. Tennyson, S. Barik, R. Szostak, E. Waks, M. F. Toney, A. F. Nogueira, B. R. A. Neves, M. S. Leite, *J. Phys. Chem. Lett.* **2018**, *9*, 3463.

[61] N. Li, Z. Zhu, Q. Dong, J. Li, Z. Yang, C. C. Chueh, A. K. Y. Jen, L. Wang, *Adv. Mater. Interfaces* **2017**, *4*, 1700598.

[62] Y. W. Zong, B.-L. Jian, H.-C. Hsu, *Opt. Mater. Express* **2019**, *9*, 870.

[63] D. Głowienka, F. Di Giacomo, M. Najafi, I. Dogan, A. Mameli, F. J. M. Colberts, J. Szmytkowski, Y. Galagan, *ACS Appl. Energy Mater.* **2020**, *3*, 8285.